Al-Nahrain Journal of Science
ANJS, Vol.29 (1), March, 2026, pp. 98 – 108

Dispersion Parameters and Electrical Characterization of $Cd_{1-x}Cu_xS$ Thin Films Deposited by Using AACVD Technique

Zaid Mohammed Jasim, Nahida B. Hasan, Mohsin K. Al-khaykanee

Department of Physics, College of Science, University of Babylon, Iraq

Article's Information

Received: 11.05.2025
Accepted: 11.11.2025
Published: 15.03.2026

Keywords:
Urbach Energy,
Dispersion Parameters,
SEM-EDX,
AACVD

Abstract

In this research, an aerosol-assisted chemical vapor deposition (AACVD) was successfully employed to synthesize $Cd_{1-x}Cu_xS$ ($0 \leq x \leq 1$) semiconductor thin films. The structural, morphological, and optical properties of the deposited films were systematically investigated as a function of copper concentration using energy-dispersive X-ray spectroscopy (EDX), scanning electron microscopy (SEM), and UV-Vis spectroscopy. The results demonstrated that the optical behavior of the films is strongly influenced by Cu incorporation. Specifically, an increase in CdS fraction resulted in a decrease in the Urbach energy, whereas the activation energy exhibited a progressive increase with higher CuS content.

http://doi.org/10.22401/ANJS.29.1.10
*Corresponding author: zaid543X21@gmail.com

1. Introduction

These semiconductor materials (p-type) exhibit unique characteristics that make them suitable for a wide range of modern optoelectronic applications, including nonlinear optics, visible light-emitting diodes, lasers, and next-generation high-efficiency solar cells [1–4]. The determination of optical constants and the optical band gap of $Cd_{1-x}Cu_xS$ semiconductor thin films, is essential not only for understanding the fundamental mechanisms behind these phenomena but, also for leveraging and advancing their potential industrial applications. Cadmium sulfide (CdS) thin films are well-known and widely studied materials, particularly in the field of thin-film solar cells. CdS is commonly used as the window layer in CdTe and $CuInSe_2$ heterojunction solar cells due to its high photosensitive nature and wide band gap [5–7]. The properties of CdS thin films can be finely tuned through the doping process. It is well established that the conductivity of pure CdS originates from native defects such as sulfur vacancies and cadmium interstitials [8]. Consequently, it is possible to control the conductivity of CdS by introducing appropriate dopants. Aerosol-assisted chemical vapor deposition (AACVD) is a technique in which a precursor solution is atomized into fine droplets, which are then carried by a hot air stream through a mobile nozzle into a heated reaction zone where chemical reactions take place [9]. Due to its low instrumentation cost and its versatility in solid-state research applications, the AACVD technique is gaining increasing popularity [10]. Thereby enabling in-house fabrication of coatings using customized enabled equipment. AACVD facilitates both research and application development in academic and industrial settings. For instance, Monárrez et al. used this technique to synthesize magnetite nanoparticles in a carrier gas reactor [11]. However, to obtain thin films, the precursor solution must be nebulized and transported to the substrate via a carrier gas and nozzle.

2. Experimental procedures

A solution of 0.05M cadmium chloride hydrated ($CdCl_2 \cdot H_2O$, MW = 201.32 g/mol) and 0.05 M of thiourea (CH_4N_2S, MW = 76.12 g/mol) were used as cadmium and sulfide sources, respectively, and 0.05 M of copper chloride hydrated ($CuCl_2 \cdot H_2O$, MW = 152.46 g/mol) (All materials were obtained from Aldrich Chemical Company, Inc). In the case of composite with Cu, a calculated amount of copper chloride hydrated was added (x=1, 0.75, 0.5, 0.25 and 0). The solution is transferred to an ultrasonic aerosol generator (nebulizer) to convert it into fine droplets. It uses tubes to deliver the aerosol to the deposition

chamber, ensuring that the droplets do not condense before reaching the substrate. The main advantage of AACVD process is its simplicity and low cost. The glass substrate was positioned on a hot plate, and an ultrasonic nebulizer was employed to generate an aerosol from the precursor solution for thin-film deposition, then the produced aerosol was delivered into the reaction chamber through a hose. The substrate, maintained on a heater at a temperature of 300 ± 20 °C, facilitated the thermal decomposition of the precursor upon reaching a stable temperature, resulting in the formation of a thin film. The entire deposition process was completed within approximately 45 minutes. An ultrasonic nebulizer was used to form an aerosol from the material to be deposited and to form thin films, and the aerosols were transferred from a device by a hose to the chamber. This chamber contains a heater, as well as two openings, one for entering the material to be deposited and the other exit of unwanted products and easy passage of the fumigant.

3. Result and Discussion

3.1. Structural properties

The scanning electron microscopy (SEM) images of the $Cd_{1-x}Cu_xS$ thin films are presented in Figure 1. The images reveal that the grains are regularly distributed across the film surface, with some defects and localized accumulations of material in certain areas, while other regions remain sparse where grain aggregation is observed, the grains form spherical clusters due to the interaction and merging of particles influenced by the evaporation and deposition conditions on the substrates. The CuS thin films consist of nanocrystalline grains that are homogeneously distributed and well-structured, as demonstrated by the micrographs. The grains exhibit strong adhesion, characterized by uniform, dense, spherical shapes without cracks. As the CdS concentration increases, the SEM images clearly show an enlargement in grain size and a shift in the preferred growth orientation of the films. These SEM observations corroborate the X-ray diffraction results, indicating that increasing the CdS volume percentage leads to a change in particle growth direction and an increase in crystallite size.

Energy-dispersive X-ray spectroscopy (EDX) was employed to analyze the elemental composition of the samples through the emitted X-rays. This technique is a highly effective tool for the micro analysis of elemental compounds and confirmed that all deposited films contained the expected elements. In addition, trace amounts of impurities, such as carbon (C) and nitrogen (N), were detected, which likely originated during the sample preparation process, as summarized in Table 1. Figure 2 illustrates the EDX spectrum of the CuS thin film, showing a strong presence of Cu and S, along with minor peaks of other elements. Figures 3, 4, and 5 present the EDX spectra of $Cd_{1-x}Cu_xS$ thin films, confirming the presence of Cu, Cd, and S, as well as other elements. The EDX spectrum of the pure CdS thin film is shown in Figure 6, where Cd and S are prominently detected alongside other minor elements. The two peaks observed for cadmium in the EDX analysis are attributed to electron transitions between different energy levels within the atom. The more intense peak (K_α) corresponds to the transition of an electron from the L-shell to the K-shell, while the less intense peak (K_β) corresponds to a transition from a higher shell to the K-shell. Furthermore, slight shifts in the positions of these peaks may occur due to the chemical environment of the sample, such as the interaction of cadmium with other elements, which alters the electron energy required for X-ray emission. These phenomena are entirely normal in EDX analysis and provide valuable insight into the chemical state of the element within the sample [13, 14].

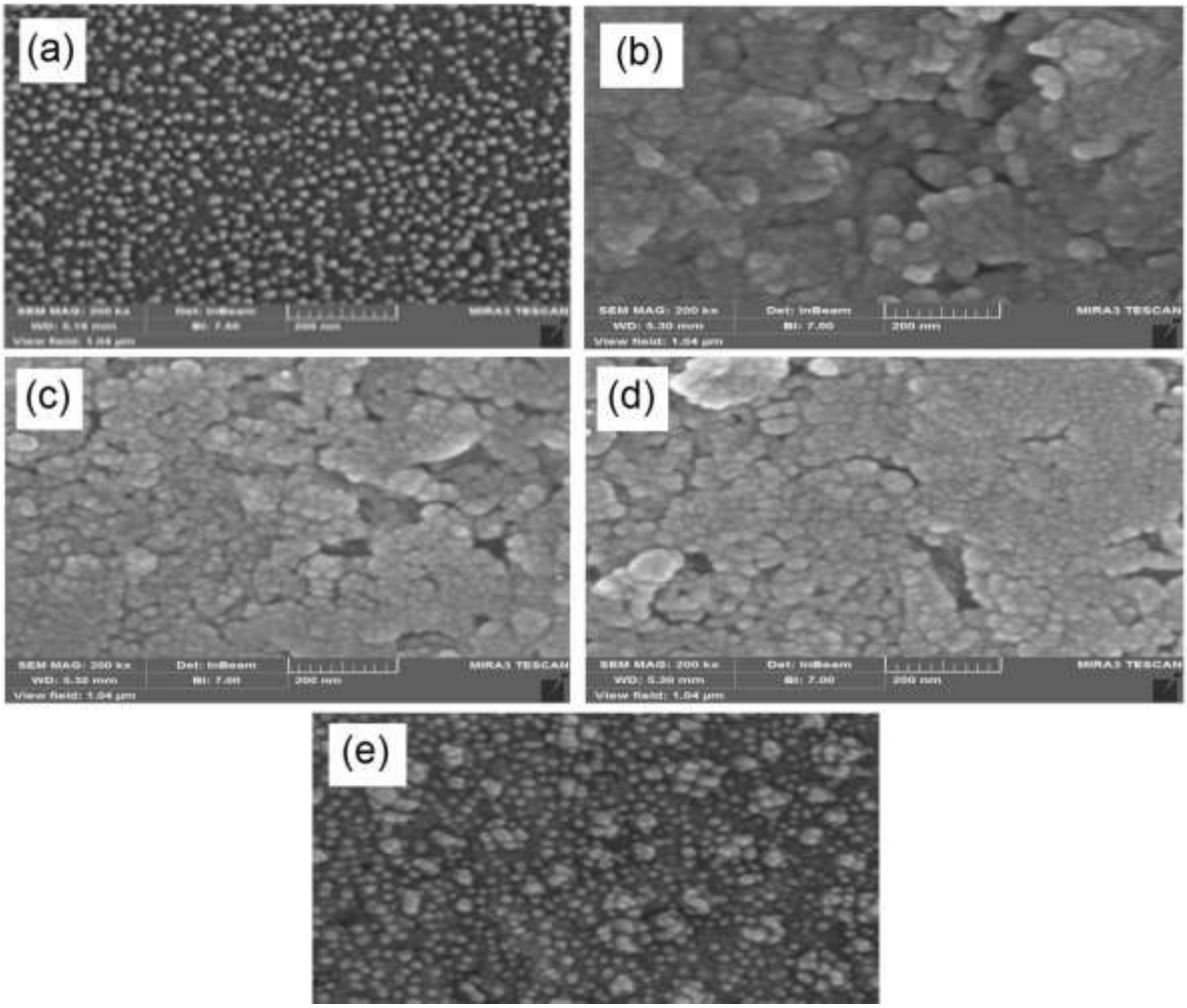

Figure 1: The SEM image of the prepared thinfilms: (a) CuS_{pure}, (b) $Cd_{0.25}Cu_{0.75}S$, (c) $Cd_{0.5}Cu_{0.5}S$,(d) $Cd_{0.75}Cu_{0.25}S$ and (e) CdS_{pure}.

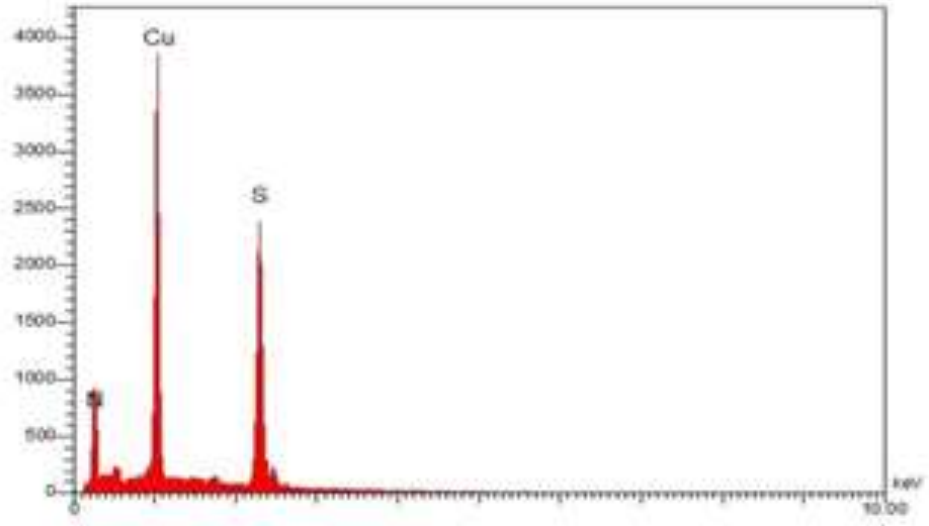

Figure 2: EDX spectrum of the prepared pure CuS thin film

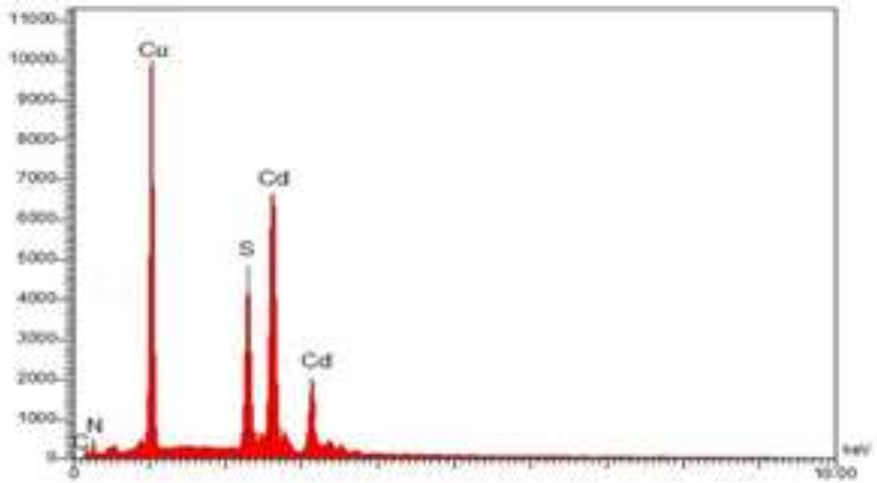

Figure 3: EDX spectrum of the prepared $Cd_{0.25}Cu_{0.75}S$ thin film

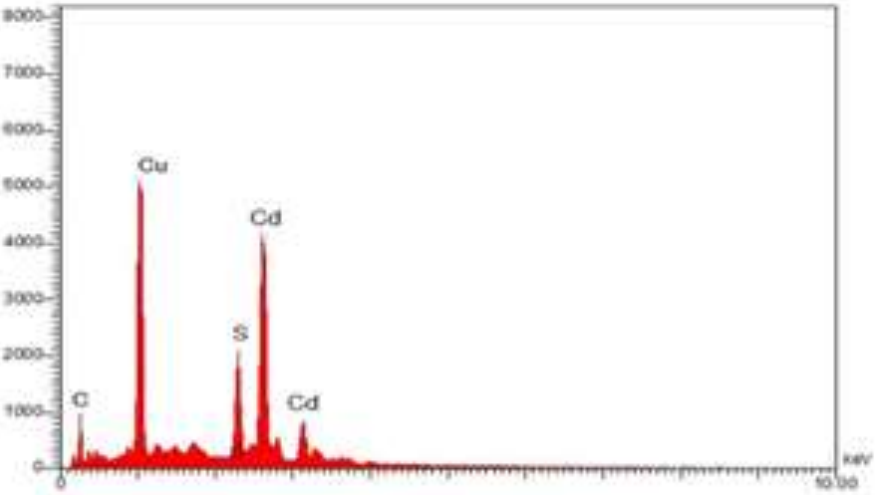

Figure 4: EDX spectrum of the prepared $Cd_{0.5}Cu_{0.5}S$ thin film.

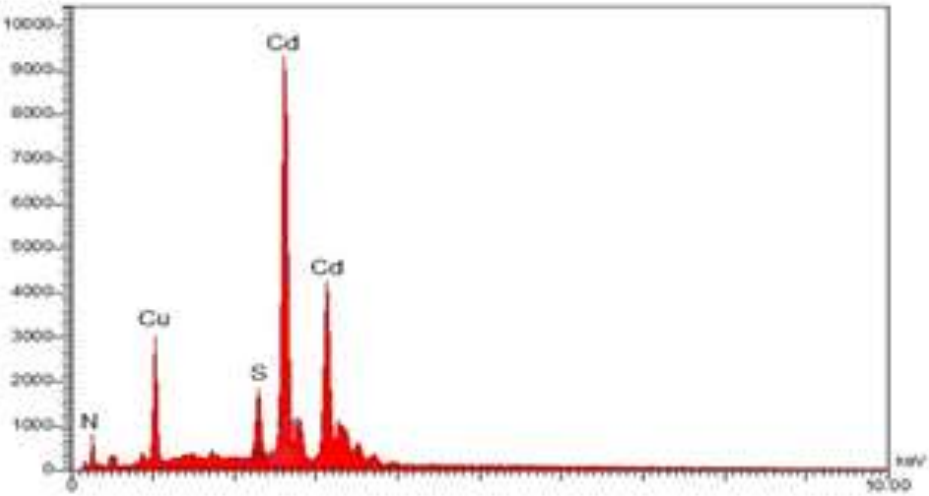

Figure 5: EDX spectrum of the prepared $Cd_{0.75}Cu_{0.25}S$ thin film

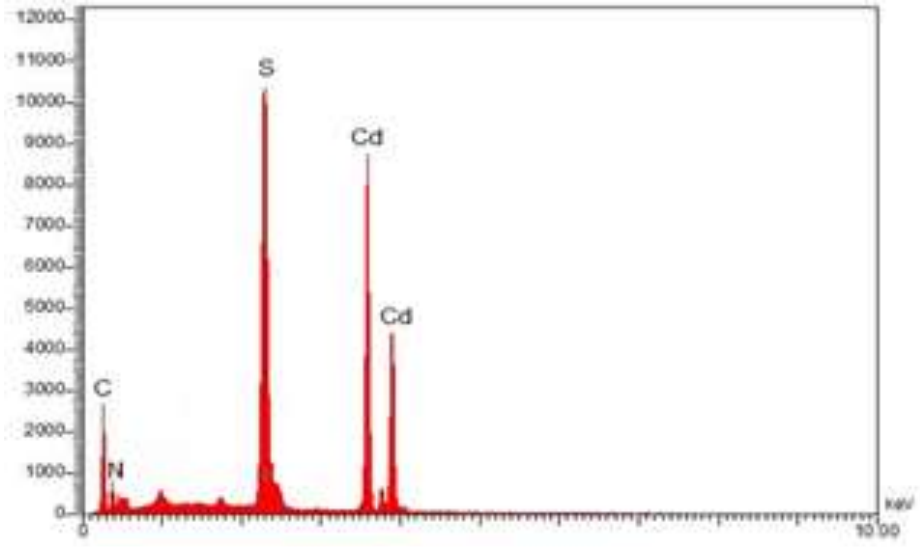

Figure 6: EDX spectrum of the prepared pure CdS thin film

Table 1: Percent compound of the ($Cd_{1-x}Cu_xS$) thin films.

Sample	Compound percentage (%)				
	Cd	Cu	S	C	N
CuS	0	49.96	41.65	0	8.39
$Cd_{0.25}Cu_{0.75}S$	29.98	41.40	17.83	1.97	2.81
$Cd_{0.5}Cu_{0.5}S$	34.68	35.71	23.84	5.76	0
$Cd_{0.75}Cu_{0.25}S$	54.52	30.10	13.51	0	1.86
CdS	49.89	0	41.85	6.46	1.79

3.2. The Urbach energy and Dispersion parameters

The band-tail width is a portion with an exponent shape at the absorption edge. According to the Urbach assumption, the magnitude of this band-tail width, also known as Urbach's energy (E_U), corresponds to the energy of the localized states created in the prohibited gap. The following equation [15, 16] gives the expression for the absorption coefficient according to Urbach's law.

$$\alpha = \alpha_{\circ} exp^{\frac{h\nu}{E_u}} \quad \ldots(1)$$

where α° is a constant, E_U is the Urbach energy, which describes the slope of the exponential edge. The E_U values are produced by charting the relationship between lnα and photon energy (hυ) as shown in Figure 7. The slope value represents the Urbach energy. Table 3 shows these values. The absorption in this area is caused by the transitions between extended states in one band and confined states in the exponential tail of the other band. The Urbach energy in CdS thin films dropped as the In-content increased, as seen in the Table 2.

Electronic transitions between localized states may account for the optical absorption coefficient's dependency on photon energy. The density of these states decreases exponentially with energy, which is consistent. The theory of Tauc [16] equation 1

$$\alpha = \alpha_{\circ} exp^{\frac{\beta h\nu}{k_B T}} \quad \ldots(2)$$

ß is called steepness parameter, The width of the absorption edge, E_U, is related to the slope of equation 2, and the ß parameter is found as $ß = k_BT/E_U$. The ß values were calculated using this relationship and taking T = 307 K, and are given in Table (2). The ß values suggest that the absorption edge changes with different (x) for ($Cd_{1-x}Cu_xS$) films.

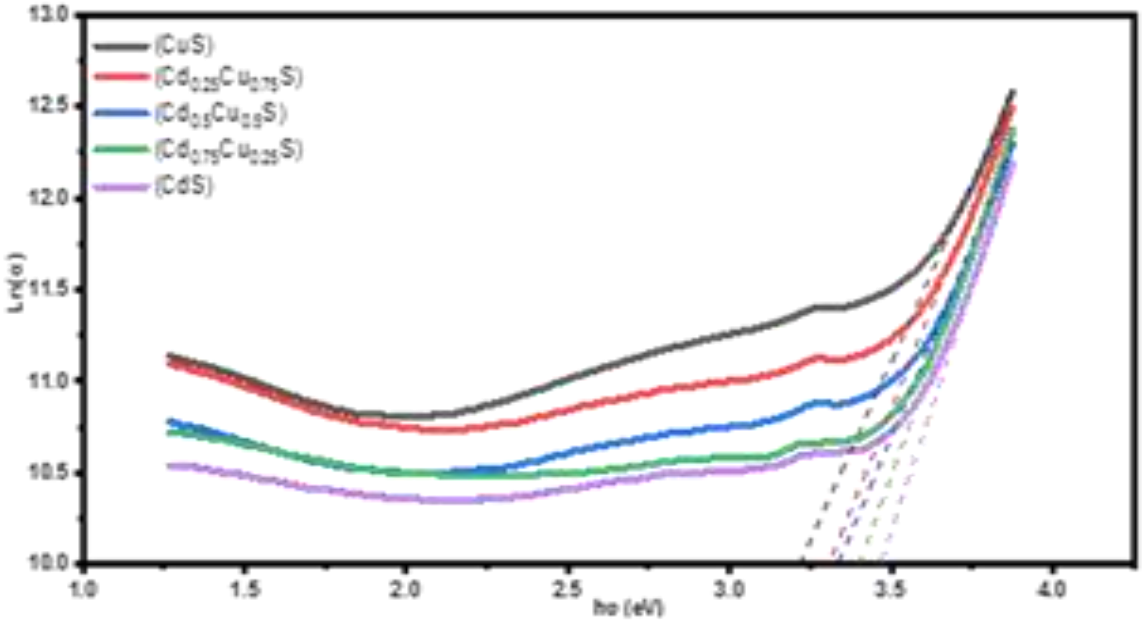

Figure7: Lnα versus (hυ) of $Cd_{1-x}Cu_xS$ thin films at different Vol.% of (x).

Table 2: The Urbach energy of $Cd_{1-x}Cu_xS$ thin films at different Vol.% of (x).

sample	E_u (meV)	$ß = k_BT/E_U$
CuS	287	0.092174878
$Cd_{0.25}Cu_{0.75}S$	246	0.107537358
$Cd_{0.5}Cu_{0.5}S$	239	0.110686987
$Cd_{0.75}Cu_{0.25}S$	202	0.130961337
CdS	214	0.12361771

The scientists Wemple and Di Domenico define the refractive index dispersion for crystalline and amorphous materials as [16]:

$$n^2 - 1 = \frac{E_\circ E_d}{E_\circ^2 - E^2} \quad \ldots(3)$$

$$\frac{1}{n^2 - 1} = \frac{E_\circ}{E_d} - \frac{E^2}{E_\circ E_d} \quad \ldots(4)$$

where n is the real part of the refractive index, hu is the photon energy, Eo is the single oscillator energy related to an average band gap and corresponds to the distance between the "centers of gravity" of the valence and conduction bands, and Ed is the dispersion energy, which measures the strength of inter-band optical transitions. This model represents the dielectric response to transitions that occur below the optical gap.

By plotting $(n^2\text{-}1)^{-1}$ vs $(hu)^2$ and fitting a straight line, the values of the parameters E_o and Ed were calculated from (E_o/ E_d) represents the intercept on the vertical axis and $(E_oE_d)^{-1}$ is the slope of the plot [16], this shown in Figure 8.

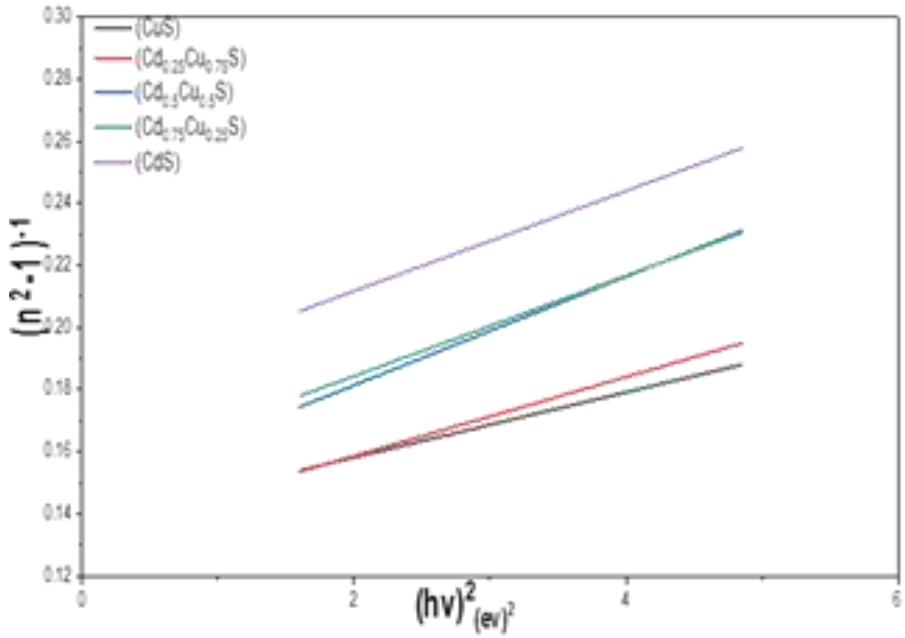

Figure 8: $(n^2-1)^{-1}$ versus $(h\upsilon)^2$ of $Cd_{1-x}Cu_xS$ thin films at different Vol.% of (x).

The refractive index dispersion can also be described by the phrase Sellmeier dispersion relation, as shown in [15].

$$n^2 - 1 = \frac{A_\circ \lambda^2}{\lambda_\circ^2 - \lambda^2} \quad \dots (5)$$

$$\frac{1}{n^2-1} = \frac{1}{A_\circ} - \frac{\lambda_\circ^2}{A_\circ \lambda^2} \quad \dots (6)$$

where λ_o is the average oscillator wavelength and it is related to the energy at which direct inter band electron transitions take place. A_o is the average oscillator strength. Linear fit of $(n^2-1)^{-1}$ versus λ^{-2} can be used to find A_o and λ_o.

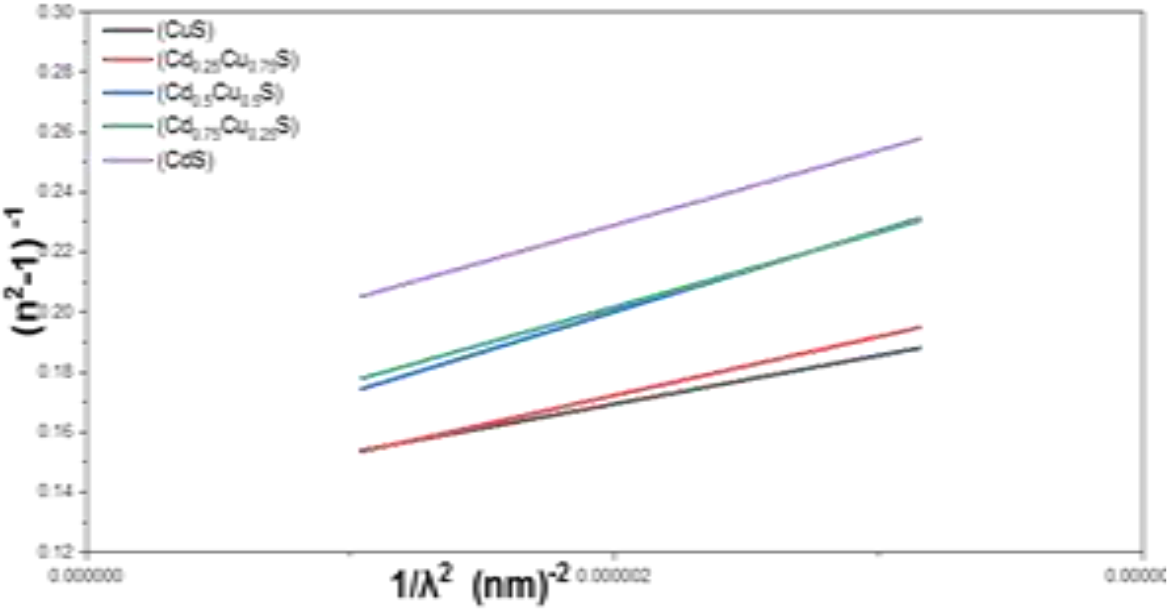

Figure9: $(n^2-1)^{-1}$ versus (λ^{-2}) of $Cd_{1-x}Cu_xS$ thin films at different Vol.% of (x).

From equations (4) and (6) are related as follows: ($A_o = E_d/E_o$) and ($\lambda_o = hc/E_o$), where h is the Plank's constant and (c) is the light velocity in vacuum.

Table 3: Dispersion parameters of of $Cd_{1-x}Cu_xS$ thin films at different (x) (from Eq. 4)

Intercept=E_o/E_d	Slope=$(E_oE_d)^{-1}$	E_d (ev)	E_o (eV)	M_{-1}(eV) $^{-2}$	M_{-3}(eV) $^{-2}$	λ_o nm
0.13716	0.0105	26.35067	3.614257	7.290755	0.558129	343.0857
0.13319	0.0105	26.7405	3.561567	7.508071	0.591897	348.1613
0.14645	0.01748	19.76444	2.894503	6.828269	0.81501	428.3983
0.15204	0.01616	20.17439	3.067314	6.577217	0.699078	404.2625
0.17948	0.01612	18.59129	3.336764	5.571651	0.500418	371.6175

Table 4: Dispersion parameters of of $Cd_{1-x}Cu_xS$ thin films at different (x) (from Eq. 6)

intercept=$1/A_o$	slope=(λ_o^2/A_o)	$A_o=E_d/E_o$	λ_o nm	E_o	E_d
0.13716	16139.11	7.290755	343.0252	3.614895	26.35531
0.13319	19553.9	7.508071	383.1606	3.236241	24.29792
0.14645	26876.88	6.828269	428.3953	2.894523	19.76458
0.15204	24849.58	6.577217	404.2785	3.067193	20.17359
0.17948	24791	5.571651	371.6542	3.336435	18.58945

3.3. Electrical properties

Figure 10 depicts the electrical conductivity as a function of temperature of ($Cd_{1-x}Cu_xS$) thin films deposited on glass. It is observed that conductivity rose with temperature, which appears to be a normal behavior as one of the semiconductor features, due to the increasing carrier concentration with temperature, yet conductivity rises with increasing copper [17]. It is quite beneficial to identify the extrinsic activation energies of impurity centers and the intrinsic main energy gap. Equation 7 depicts the (Ln σ) vs. reciprocal of the absolute temperature (10^3/T), allowing us to determine the activation energy by measuring the slope of straight lines (-ΔE/k) [18]. Figure 11 demonstrates that there are two phases of conductivity over the rising temperature range. The first activation energy (E_{a2}) occurs at higher temperatures and is caused by the conduction of excited carriers into extended states beyond the mobility edge, whereas the second activation energy (E_{a1}) occurs at low temperatures and is caused by the transport of carriers to localized states either near valence band or in between valence and conduction band. These two conduction processes imply the existence of two transport mechanisms. Furthermore, this drop implies a negative coefficient of resistance, demonstrating that the semiconductor behavior of ($Cd_{1-x}Cu_xS$) thin films is non-linear with temperature.

$$\sigma = \sigma_o \, exp\left(\frac{-E_a}{k_B \check{T}}\right) \quad \ldots (7)$$

Table 5 demonstrates that the value of E_{a2} is greater than the value of E_{a1}. This indicates that the electrical conductivity of the material is temperature-dependent, following the relation $\sigma \propto T^{3/2}$[18].

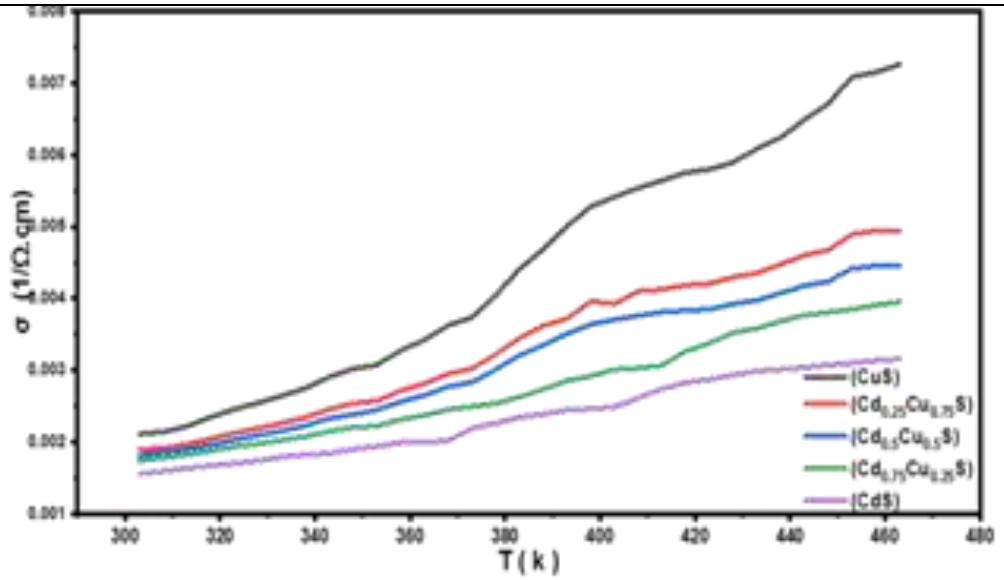

Figure 10: Variation of $\sigma_{D.C}$ versus temperature for ($Cd_{1-x}Cu_xS$) films at different Vol.% of (x).

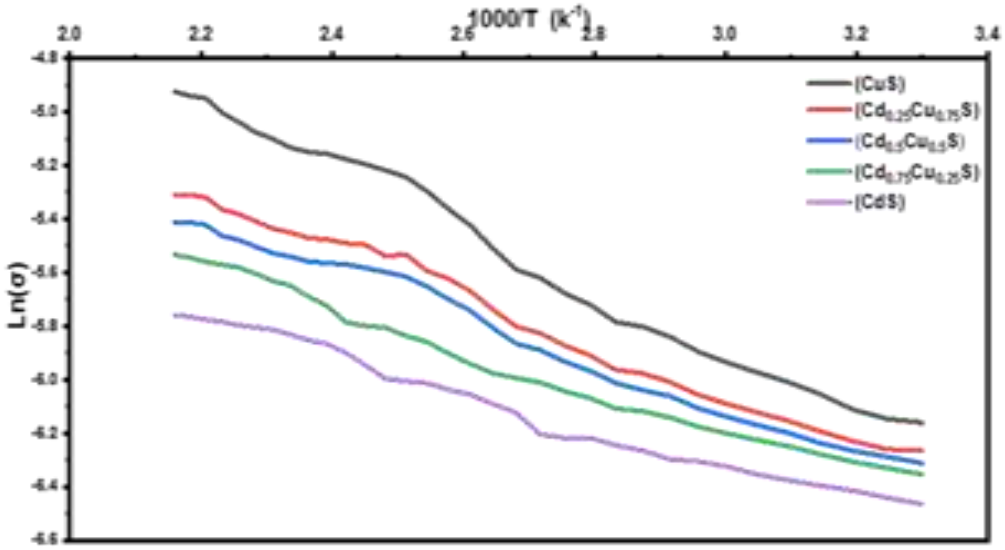

Figure 11: Ln σ versus 1000/T for ($Cd_{1-x}Cu_xS$) thin films at different Vol.% of (x).

The Hall coefficient (R_H) is significant for understanding electrical characteristics since it is dependent on the value of the incoming magnetic field on the film that is situated vertically in front of it. Hall Effect studies of deposited samples from x = (1 to 0) revealed p-type conductivity, resulting in positive RH values. Table 6 provides estimates for charge carrier type, concentration (n_H), Hall mobility (μ_H), conductivity (σ), and resistivity (ρ) based on Hall measurements. According to the table, the Hall coefficient and carrier mobility decrease with increasing CuS content, whereas both the electrical conductivity and carrier concentration increase. This behavior is attributed to the higher charge carrier density, which reduces the energy gap between the Fermi level and the conduction band edge [19]. Consequently, the activation energy rises as the CuS mixing ratio increases. Moreover, increasing the CuS volume fraction led to higher conductivity (σ), likely due to modifications in the thin film structure, including increased grain size and enhanced potential barriers at the grain interiors. These changes result in the trapping of charge carriers at grain boundaries, thereby reducing dispersion [19].

Table 5: D.C. conductivity parameters for ($Cd_{1-x}Cu_xS$) thin films at different Vol.% of (x).

Sample	E_{a1} (eV)	Temp.Range(K)	E_{a2}(eV)	Temp.Range(K)	σ At T=393 (K)$(\Omega.cm)^{-1}$
CuS	0.0802	(303-373)	0.0973	(373-463)	0.0050
$Cd_{0.25}Cu_{0.75}S$	0.0661	(303-373)	0.0973	(373-463)	0.0037
$Cd_{0.5}Cu_{0.5}S$	0.0623	(303-373)	0.0728	(373-463)	0.0035
$Cd_{0.75}Cu_{0.25}S$	0.0501	(303-373)	0.066	(373-463)	0.0028
CdS	0.0397	(303-373)	0.0635	(373-463)	0.0024

Table 6: Hall parameters for ($Cd_{1-x}Cu_xS$) films at different Vol.% of (x) at room temperature.

Sample	R_H(cm^3 / C)	n_H(1 / cm^3)	$\sigma_{R.T}(\Omega.cm)^{-1}$	$\rho_{R.T}(\Omega.cm)$	$\mu_H(cm^2/V.s)$
CuS	1.413×10^{5}	1.538×10^{14}	1.123×10^{-5}	0.89×10^{5}	0.41×10^{1}
$Cd_{0.25}Cu_{0.75}S$	1.759×10^{5}	9.514×10^{13}	1.063×10^{-5}	0.94×10^{5}	0.72×10^{1}
$Cd_{0.5}Cu_{0.5}S$	2.071×10^{5}	7.816×10^{13}	0.980×10^{-5}	1.02×10^{5}	0.96×10^{1}
$Cd_{0.75}Cu_{0.25}S$	2.279×10^{6}	5.043×10^{12}	0.869×10^{-5}	1.15×10^{5}	1.03×10^{1}
CdS	2.501×10^{6}	2.602×10^{12}	0.757×10^{-5}	1.32×10^{5}	1.31×10^{1}

4. Conclusions

Energy dispersive X-ray spectroscopy confirmed the presence of the main components in the $Cd_{1-x}Cu_xS$ thin films, with only minor impurities such as nitrogen (N) and carbon (C), likely appeared during preparation. Elemental mapping indicated a homogeneous distribution of elements. Scanning electron microscopy images revealed a surface morphology composed of oval-shaped nanoparticles distributed regularly across the film surface, with some localized defects and grain aggregations forming spherical clusters due to deposition conditions. The grains exhibited strong adhesion, being uniform, dense, and crack-free. Increasing the CdS concentration resulted in an enlargement of grain size and a shift in growth orientation. These SEM observations are consistent with X-ray diffraction findings, which showed an increase in crystallite size and changes in growth direction as the CdS volume fraction increased. A strong correlation was observed between nanostructure features such as grain size and porosity and the electrical conductivity of the films. Smaller grains potentially improve charge transfer by providing a larger surface area. EDX analysis confirmed the presence of all the expected elements in the thin films. Hall Effect measurements confirmed that the charge carriers are p-type. Electrical conductivity exhibited strong temperature dependence, showing semiconductor-like behavior characterized by an increase in conductivity with rising temperature.

Acknowledgments: The authors are deeply indebted to the administration of the Department of Physics, College of Science, University of Babylon, Iraq

Funding Statement: No funding is received for this work.

Conflicts of Interest: The authors declare no conflict of interest pertaining this work.

References

[1] Wondmagegn, W.; Marandi, M.; Saievar-Iranizad, E.; Taghavinia, N.; Liu, B.; Sun, H. D.; "CdS thin film transistor for inverter and operational amplifier circuit applications". Microelectron. Eng., 157: 64–70, 2016.

[2] Molaei, M.; Marandi, M.; Saievar-Iranizad, E.; Taghavinia, N.; Liu, B.; Sun, H. D.; Sun, X. W.; "Near-white emitting QD-LED based on hydrophilic CdS nanocrystals". J. Lumin., 132: 467–473, 2012.

[3] Li, P.; Wang, Y.; Zhang, Y.; Wang, X.; "TiO_2 activity enhancement through synergistic effect of photons localization of photonic crystals and the sensitization of CdS quantum dots". Photon. Nanostruct.-Fundam. Appl., 23: 12–20, 2017.

[4] Wang, F.; Liang, L.; Chen, K.; Sun, J.; "CO_2 induced template approach to fabricate the porous C/CdS visible photocatalyst with superior activity and stability". J. Mol. Catal. A Chem., 425: 76–85, 2016.

[5] Sharma, A.; Kumar, R.; Bhattacharyya, B.; Husale, S.; "Hot electron induced NIR detection in CdS films," Sci. Rep., 6: 22939, 2016.

[6] Adem, K.; "Electronic Properties of PbTe/Si Heterojunction". Al-Nahrain J. Sci., 15(4): 129–133, 2012.

[7] Camacho-Espinosa, E.; Rejón, V.; Hernández-Rodríguez, E.; Mis-Fernández, R.; "$CHClF_2$ gas mixtures to activate all-sputtered CdS/CdTe solar cells". Sol. Energy, 144: 729–734, 2017.

[8] Ghosh, B.; Das, M.; Banerjee, P.; Das, S.; "Fabrication of vacuum-evaporated SnS/CdS heterojunction for PV applications". Sol. Energy Mater. Sol. Cells, 92: 1099–1104, 2008.

[9] Hincapié-Zapata, J. M.; Castrillón-González, E. Y.; Cruz-Muñoz, B.; Medina-Barreto, M. H.; Dorantes-Rodríguez, R. J.; "Instrumentation and control of an aerosol-assisted chemical vapor deposition system (AACVD) ". Dyna, 86(210): 52–57, 2019.

[10] Choy, K. L.; "Chemical vapour deposition of coatings". Prog. Mater. Sci., 48(2): 57–170, 2003.

[11] Monárrez-Cordero, B. E.; Amézaga-Madrid, P.; Sáenz-Trevizo, A.; Pizá-Ruiz, P.; Antúnez-Flores, W.; Miki-Yoshida, M.; "Synthesis and characterization of composite Fe-Ti oxides nanoparticles with high surface area obtained via AACVD". Ceram. Int., 44(6): 6990–6996, 2018.

[12] Ahmed, M.; Bakry, A.; Dalir, H.; Shaaban, E. R.; "Copper effect on cadmium sulfide thin films for spintronics: microstructures, morphological, photoluminescence and magnetic properties". J. Mater. Sci. Mater. Electron., 19(11): 785–792, 2022.

[13] Goldstein, J. I.; Newbury, D. E.; Michael, J. R.; Ritchie, N. W. M.; Scott, J. H. J.; Joy, D. C.; "Scanning electron microscopy and X-ray microanalysis". In Scanning Electron Microscopy and X-ray Microanalysis, 4th ed.; Springer, New York, USA, pp. 1–832, 2018.

[14] Reimer, L.; "Physics of image formation in scanning electron microscopy". In Scanning Electron Microscopy: Physics of Image Formation and Microanalysis, 2nd ed.; Springer, Berlin, Germany, pp. 1–435, 1998.

[15] Hassan, N. B.; "Dispersion Parameters and Morphology of Chemical Spray Pyrolysis Deposited Fe_2O_3 Thin Films Prepared at Different Thickness". Indian J. Appl. Res., 3(6): 449–452, 2011.

[16] El-Zaiat, S. Y.; El-Den, M. B.; El-Kameesy, S. U.; El-Gammam, Y. A.; "Spectral dispersion of linear optical properties for Sm_2O_3 doped B_2O_3–PbO–Al_2O_3 glasses". Opt. Laser Technol., 44(5): 1270–1276, 2012.

[17] Kamruzzaman, M.; Runa, T.; Podder, J.; Anowar, M. G. M.; "Synthesis and Characterization of $Cd_{1-x}Cu_xS$ Thin Films Prepared Using the Spray Pyrolysis Technique". Semicond. Sci. Technol., 27(3): 035017, 2012.

[18] Farag, A. A.; Ibrahim, M. A.; Ismail, F. M.; "Electrical and optical properties of sprayed CdS thin films". Chalcogenide Lett., 6(12): 267–276, 2009.

[19] Diliegros-Godines, C. J.; Lombardero-Juárez, D. I.; Machorro-Mejía, R.; González, R. S.; Pal, M.; "Electrical properties and spectroscopic ellipsometry studies of covellite CuS thin films deposited from non-ammoniacal chemical bath". Opt. Mater., 91: 147–154, 2019.